

## Research Article

# The Analysis of Biomimetic Caudal Fin Propulsion Mechanism with CFD

Guijie Liu <sup>1,2</sup>, Shuikuan Liu,<sup>1,2</sup> Yingchun Xie <sup>1,2</sup>, Dingxin Leng,<sup>1,2</sup> and Guanghao Li<sup>1,2</sup>

<sup>1</sup>Department of Mechanical and Electrical Engineering, College of Engineering, Ocean University of China, Qingdao 266100, China

<sup>2</sup>Key Laboratory of Ocean Engineering of Shandong Province, Ocean University of China, Qingdao 266100, China

Correspondence should be addressed to Yingchun Xie; [xiyec@ouc.edu.cn](mailto:xiyec@ouc.edu.cn)

Received 27 July 2019; Revised 22 January 2020; Accepted 25 February 2020; Published 24 June 2020

Academic Editor: Mohammad Rahimi-Gorji

Copyright © 2020 Guijie Liu et al. This is an open access article distributed under the Creative Commons Attribution License, which permits unrestricted use, distribution, and reproduction in any medium, provided the original work is properly cited.

In nature, fish not only have extraordinary ability of underwater movement but also have high mobility and flexibility. The low energy consumption and high efficiency of fish propulsive method provide a new idea for the research of bionic underwater robot and bionic propulsive technology. In this paper, the swordfish was taken as the research object, and the mechanism of the caudal fin propulsion was preliminarily explored by analyzing the flow field structure generated by the swing of caudal fin. Subsequently, the influence of the phase difference of the heaving and pitching movement, the swing amplitude of caudal fin, and Strouhal number (St number) on the propulsion performance of fish was discussed. The results demonstrated that the fish can obtain a greater propulsion force by optimizing the motion parameters of the caudal fin in a certain range. Lastly, through the mathematical model analysis of the tail of the swordfish, the producing propulsive force principle of the caudal fin and the caudal peduncle was obtained. Hence, the proposed method provided a theoretical basis for the design of a high-efficiency bionic propulsion system.

## 1. Introduction

Autonomous underwater vehicles (AUVs) are a type of marine equipment that play a significant role in improving the daily life of human beings, such as to monitor the marine environment or safeguard modern military operations. Thus, it is gradually becoming an extensive research topic both at home and abroad [1]. However, AUVs have some shortages, which greatly limit the application in the narrow, complex, and dynamic environment. For instance, the propulsive efficiency is low. Moreover, maneuvering performance and concealment are poor and they have a negative influence on environment.

In nature, fish evolved into the swimming mechanism that has an outstanding capability to produce high thrust efficiently and gains high performance in maneuvering flexibility and controllability. Recently, interest in the motion of fish has increased. A lot of attempts have been made to mimic the motion of fish and apply it to underwater vehicles and robots in the field of oceanography [2].

The most effective movements of swimming aquatic animals of almost all sizes appear to have the form of a transverse wave progressing along the body from fish head to fish tail [3], and the fishes that have faster speed are using the biomimetic caudal fin propulsion way. They have a high hydrodynamic efficiency and are applicable to long-time, long-distance swimming in this way [4]. However, the study of its hydrodynamic characteristics has not come to a unified conclusion.

Early in 1970s, Lighthill [5, 6] employed the influence of the swing of the caudal fin on the flow field according to the “slender body theory” and then came up with “large-scale slender body theory” that is more suitable for analyzing fish propulsion patterns. Until 2011, Candelier et al. [7] extended the “slender body theory” to a three-dimensional case to obtain the pressure expression and momentum expression of the slender fish body.

The above researchers made large contributions to establish and develop the “slender body theory.” There is no denying that the theory laid solid foundation for exploring the

propulsion mechanism of fish. Caudal fin is one of the most important parts in fish body to generate a propulsive force. As the simplest propulsive mode of fish, caudal fin swing propulsive has been concerned by extensive researchers since the beginning of the last century. The first to study the relationship between the parameters of the caudal fin swing and the propulsive force was the “resistance hydrodynamic model” established by Taylor in 1952 [8], which was applicable to low Reynolds number.

As our country keeps a watchful eye to the marine resources, more and more scientific institutions have begun to do research work in the field of caudal fin propulsion and have made certain achievements. The influence of caudal fin stiffness [9, 10], caudal fin area [11], fin strip movement [12], and swing phase [13] on caudal fin propulsion, velocity, and efficiency has been preliminarily studied by researchers. Besides, Liu et al. [14] considered different thrusts at different frequencies and found that they had a specific optimum frequency under a specific flexible connection. Xin and Wu [15] studied the effect of the shape of caudal fin on swimming speed and efficiency in fish free propulsion and found that the shape of the optimal caudal fin varies with different swimming modes. Tomita et al. [16] clarify developmental processes of the white shark caudal fin, based on morphological observations of the caudal fin over several developmental stages.

The above researchers mainly explored the relationship between various influencing factors in theory, and some researchers have studied the advancement of fish by establishing a physical model and combining theory with experiment [17, 18]. In 2016, Yin et al. [19] took into account the thrust and resistance acting on the robot, and the thrust characteristic is an effective factor for calculating the thrust. In 2018, Zhong et al. [20] considered the interaction between the pectoral fin and the caudal fin, founding that the dynamics of the pectoral fin and the caudal fin can be used to estimate the overall swimming speed of the biomimetic fish.

At present, few studies have been carried out on the shape of caudal fin and its propulsion principle of swordfish. For the sake of bridging this research gap, in this paper, the key parameters of caudal fin were firstly calculated by using dynamic mesh technology in Fluent software. The generation of eddy currents and the generation of anti-Karman vortex streets were analyzed. Secondly, by changing the major parameters of the caudal fin, the propulsion mechanism was explored. Finally, through the study of the movement law of the fish tail, the biomimetic mechanism is fitted to the movement, which is verified to be correct and reasonable. Meanwhile, the mechanism of the propeller force during the propulsion process is further explored. By using the linkage, the caudal peduncle was fitted by a bionic method, which laid the foundation for the underwater robots to realize high-efficiency propulsion.

## 2. Kinematic Modelling Based on CFD

*2.1. Establishment of a Finite Element Model.* The data of caudal fin was collected by 3D scanning and reverse engineering.

Then, a three-dimensional model was imported into Solidworks software. In the software, the transverse symmetry surface of the caudal fin was sliced to obtain the transverse interface of the caudal fin. The two-dimensional calculation model of the caudal fin is shown in Figure 1.

The CFD calculation domain setting model is displayed in Figure 2. The flow field was established to be 1800 mm × 600 mm. The caudal fin has a length of 150 mm and a maximum thickness of 15 mm. The outer rectangular border is the flow field boundary. In order to ensure accuracy and control the number of meshes, a sufficient number of nodes was arranged on the profile of caudal fin to encrypt the meshes near the caudal fin, and the meshes for the flow boundary were less relative.

The boundary conditions are exhibited in Table 1, and the movement of the caudal fin model was controlled by a UDF function. The mesh model is shown in Figure 3, and the number of grids was about 31652.

*2.2. The Motion of Fish Body and Function of Fish Body Wave.* In the process of propulsion, the fish mainly relies on the fluctuations of the spine curve to generate a propulsive force. Through extensive biological observations and experimental studies of fish behavior, researchers have found that an implicit traveling wave is in the propulsive motion generated by the swinging caudal fin and the flexible body, which travels from the posterior neck to the tail. The bending of the spine and muscle tissue makes the fish appear wavy morphology, and the amplitude is gradually bigger from the fish head to the fish tail. The wave velocity of the traveling wave also known as “fish body wave” is greater than the forward speed of the fish body. The corresponding mathematical function expression is called the fish body wave function. To some extent, the fish body wave function can be seen as synthesized by the fish wave envelope and sinusoidal curve, as shown in Figure 4.

The wave function of the fish body begins from the center of the inertia force of the fish body and gradually extends to the caudal peduncle, and its curve equation [21] can be expressed as

$$y_{\text{body}}(x, t) = (c_1x + c_2x^2) \sin(kx + \omega t), \quad (1)$$

where  $y_{\text{body}}$  is the lateral displacement of the fish,  $x$  is the axial displacement of the fish,  $k$  is the multiple of wavelength ( $k = 2\pi/\lambda$ ),  $\lambda$  is the wavelength of the fish body wave,  $c_1x + c_2x^2$  is the fish wave amplitude envelope function,  $c_1$  is the primary coefficient of the fish body wave amplitude envelope,  $c_2$  is the quadratic coefficient of the fish body wave amplitude envelope, and  $\omega$  is the fish body wave frequency ( $\omega = 2\pi f$ ).

The swing amplitude of the caudal fin and the distribution of the body wave amplitude can be adjusted by adjusting the value of  $c_1$  and  $c_2$ .

*2.3. Main Parameters of Hydrodynamic Performance of Caudal Fin.* The St number is a parameter that expresses the characteristics of the wake structure [22]. It indicates the frequency of the swirl and the distance between them.

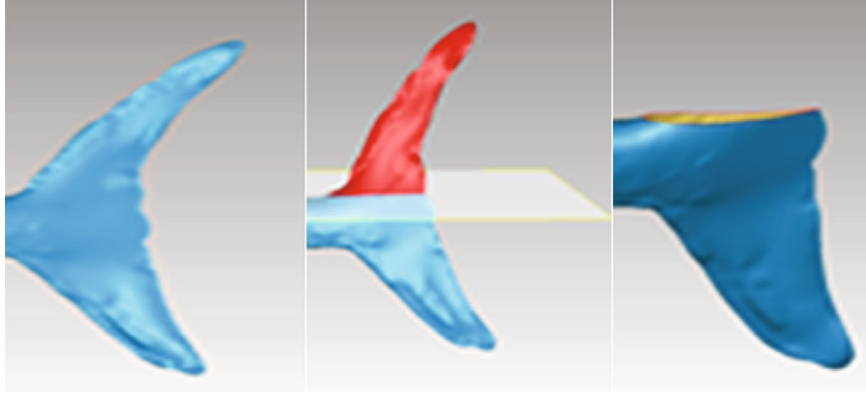


FIGURE 1: Data model of caudal fin.

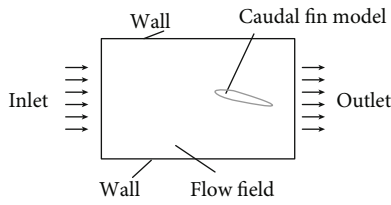


FIGURE 2: Calculation domain setting.

TABLE 1: Boundary condition setting.

	Type	Value
Inlet	Velocity-inlet	0 m/s
Outlet	Pressure-outlet	0 Pa
Upper and lower boundary	Wall	—
Caudal fin model	Wall	—

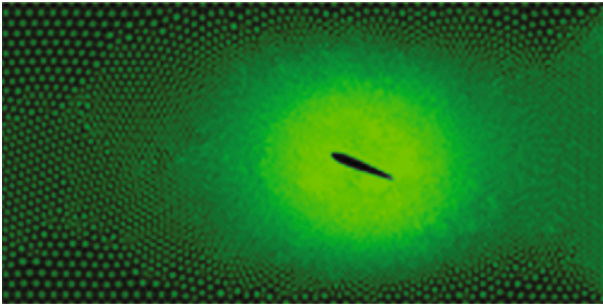


FIGURE 3: Finite element model.

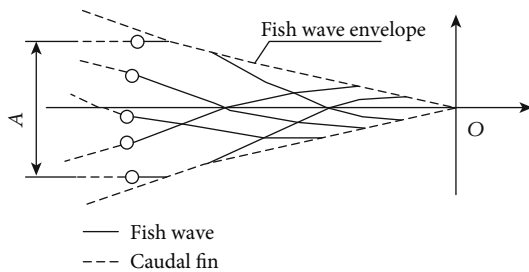


FIGURE 4: Fish body wave and fish amplitude envelope.

For the fluctuating caudal fin, the St number is calculated by the following formula:

$$St = \frac{fA}{V}, \quad (2)$$

where  $f$  represents the swing frequency of caudal fin (Hz),  $A$  represents the caudal fin heaving motion amplitude, and  $V$  is the average swimming velocity.

The angle of attack  $\delta_{\max}$  is defined as when the fins pass the equilibrium position, the angle moves between the tangential direction of the propulsive wave and the axis of symmetry of the caudal fin, which can be expressed as

$$\delta_{\max} = \phi - \theta_0, \quad (3)$$

where  $\phi$  indicates the angle between the  $X$ -axis and the tangential direction of the propulsive wave and  $\theta_0$  indicates the angle between the geometric axis of symmetry and the  $X$ -axis when the tail fin passes the equilibrium position.

**2.4. Basic Equation Based on CFD Numerical Calculation.** CFD is a numerical calculation method for solving flow control equations [23]. Considering viscous and incompressible flow, the following continuity equation and motion equation are established.

$$\frac{\partial \rho}{\partial t} + \frac{\partial}{\partial x_i} (\rho u_i) = 0, \quad (4)$$

$$\frac{\partial}{\partial t} (\rho u_i) + \frac{\partial (\rho u_i u_j)}{\partial x_j} = -\frac{\partial p}{\partial x_i} + \frac{\partial p}{\partial x_j} \left( \mu \frac{\partial u_i}{\partial z_j} - \rho \bar{u}_i' u_j' \right) + S_i, \quad (5)$$

where  $\rho$  represents the density of fluid,  $t$  represents the time,  $u_i$  represents the velocity of fluid,  $x$  is the space coordinates,  $p$  represents the fluid pressure,  $\mu$  represents the kinematic viscosity coefficient, and  $S_i$  represents the user-defined source term.

In order to solve Equations (4) and (5), it is also necessary to add a turbulent transport equation. It has been calculated that the Reynolds number of all the working conditions is

between  $4 \times 10^4$  and  $1.4 \times 10^5$ , so the standard  $k-\varepsilon$  [24, 25] model is used for calculation. It has been verified that the standard  $k-\varepsilon$  model is suitable for practical engineering flow calculations because of its high robustness and reasonable accuracy. For further solving the equations above, the coupled implicit algorithm is utilized; hence, variables such as pressure, velocity, and stress can be obtained simultaneously [26].

### 3. Hydrodynamic Calculation

*3.1. Analysis of the Mechanism of Caudal Fin Propulsion.* The fluctuation frequency  $f = 0.8$  Hz, the swing amplitude  $A = 120$  mm, the fluctuation period  $T = 1.25$  s, and the phase difference of the heaving and pitching movement  $60^\circ$  are selected for calculation [5, 13, 27].

As shown in Figure 5, when  $t = 0.01$  s, the caudal fin begins to move forward. At this time, caudal fin is around in anticlockwise rotation, and the upper side of the caudal fin fluid pressure gradually increased. Meanwhile, the lower side of the pressure becomes smaller due to the formation of a low-pressure area.

When  $t = 1/4 T$  (0.31 s), the caudal fin reaches to the highest position of the swing. The lower side of the fish tail forms a low-pressure zone, and the swirl current is generated by the front end of the caudal fin, which is the beginning of the second swirl. In  $t = 0.5$  s, the rotation of the swirl direction is counterclockwise rotation, which is opposite to the first swirl direction.

When  $t = 1/2 T$  (0.63 s), the second swirl completely falls off and the high- and low-pressure zones on both sides of the caudal fin appear mutative. The lower side is the high-pressure area, and the upper side is the low-pressure area.

$t = 1.74$  s and  $t = 1.77$  s are the fourth swirl belonging to the second cycle, and mechanism is similar with the second swirl.  $t = 2.35$  s is the fifth swirl, and it also belongs to the second cycle, the mechanism of which is similar with the third swirl.

After the analysis of the caudal fin swimming process, we can acquire that the caudal fin swims in a wave manner. On the upper and lower sides of the caudal fin, the high-pressure and low-pressure regions are formed according to the pitching direction. The forward swirl is gradually formed at the front end of the caudal fin. The swirl of the body becomes larger as the caudal fin swings. Meanwhile, the swirl moves toward the end of the caudal fin, and it finally falls off. By observing the direction of rotation of the five shedding swirls, it can be found that the first, third, and fifth swirls are below the  $X$ -axis and the direction is clockwise. The second and fourth swirls are above the  $X$ -axis, and the direction of rotation is clockwise. It can be found that these five shedding swirls are in the tangential direction of  $X$ -axis and opposite to the swimming direction of the caudal fin. And then the Karman vortex shedding is formed, forming a backward jet to result in forward thrust.

*3.2. Effects of St Number.* The operating condition is selected with the swing amplitude  $A = 120$  mm, and the phase difference is  $60^\circ$ .

As depicted in Figure 6, it can be seen that when the frequency is constant, as the  $St$  coefficient increases, the flow velocity decreases, and the magnitude of the thrust coefficient gradually becomes smaller. The lower limit of the thrust coefficient is substantially the same under any working condition because the upper limit of the thrust coefficient decreases as the  $St$  coefficient increases. When the frequency is 1 Hz, it can be seen that although the magnitude of the thrust coefficient changes with the change of the  $St$  number, the amplitude of the upper limit changes significantly. At the same time, as the frequency increases, the lower limit of the thrust coefficient also increases.

Since the caudal fin moves in the negative direction of the  $X$ -axis, the negative value in Figure 6 indicates the same propulsive force as the caudal fin move direction, and the positive value indicates the resistance.

It can be seen from Figure 7 that the variation law of the average force curve is gradually increasing with the increase of the  $St$  number, but the range of the increasing amplitude is gradually smaller. When  $St = 0.25$ , the force generated by the fins at  $f = 0.5$  Hz is not conducive to the advancement of the fish body. It can be obtained that the swing frequency has a huge influence on the thrust coefficient. The fish body can overcome the flow resistance by adjusting its own tail-end frequency in time according to water velocity to avoid the force of the caudal fin to hinder the movement.

*3.3. Effects of Phase Difference and the Angle of Attack.* During the process of fluctuation of the caudal fin, there is a phase difference between the heaving and pitching movement. The different motions can be obtained through changing the phase differences and then the hydrodynamic numerical simulation can be analyzed, respectively.

The thrust coefficient changing with times is shown in Figure 8. It can be obtained that the force of the caudal fin is the same as the direction of advancement at the beginning. The direction of force changes with the heaving and pitching movement, which becomes the opposite direction with the fish swimming, and is not conducive to fish for forward. In Figure 8, the shaded portion below the line of  $y = 0$  indicates that it is conducive to fish for moving forward while the shaded portion above the straight line of  $y = 0$  indicates that it is not conducive to fish for moving forward. The longer time it takes to promote the advancing force of the caudal fin, the more favorable to forward. Comparing Figures 8(a)–8(d), it can be seen that as the increase of the phase difference, the larger the shadow area below the  $y = 0$  line, which means the longer time to propulsion in a cycle.

As displayed in Figure 9, when the phase difference is  $50-60^\circ$  (the angle of attack is  $21.6-25.6^\circ$ ), the caudal fin is propelled by a large force, so it is a relatively optimized mode of motion in this condition.

*3.4. Effects of Swing Amplitude.* Based on above analysis, the following parameters are selected for calculation: the phase difference is  $60^\circ$ , and the angle of attack is  $23.3$ . The swing amplitude  $A$  is selected as the following values:  $A = 90$  mm,  $120$  mm,  $150$  mm,  $180$  mm, and  $210$  mm. In order to obtain



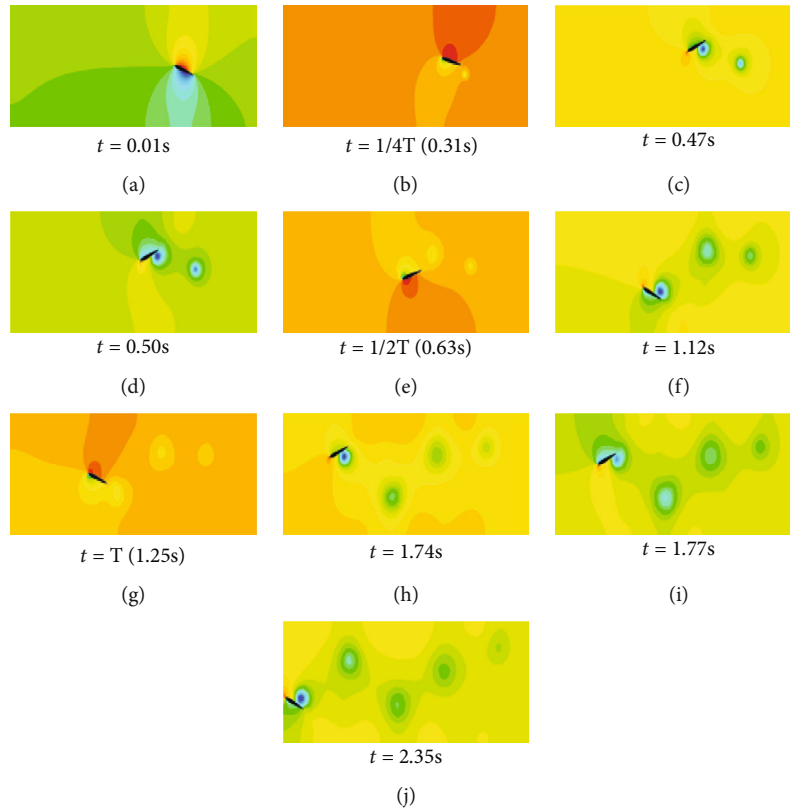


FIGURE 5: The fluid pressure distribution of the fluctuation caudal fin at different times.

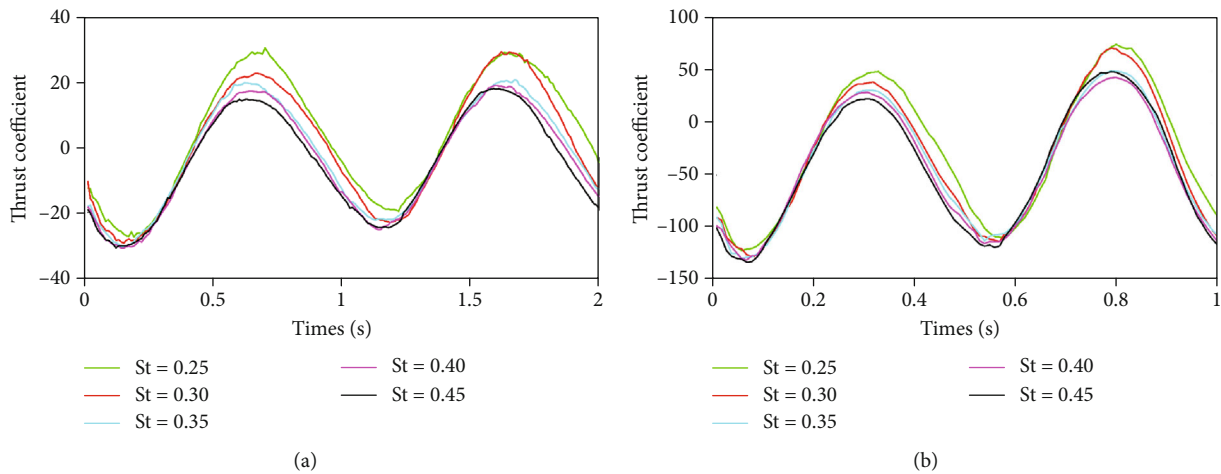


FIGURE 6: Forced condition of different values of St: (a)  $f = 0.5$  Hz; (b)  $f = 1$  Hz.

the relationship between the thrust coefficient and the swing amplitude intuitively, Figure 10 was drawn.

As shown in Figure 10, it can be seen that as the swing amplitude increases, the propulsion force of the caudal fin in the swimming direction increases. When the swing frequency is  $f = 0.8$  Hz and the swing amplitude is 90 mm and 120 mm, the swing of the caudal fin will generate a force that hinders the advancement of the fish body. When the swing amplitude is larger than 150 mm, the propulsive force for promoting motion will be generated. In addition, comparing the two curves, it can be seen that when the

swing amplitude is 180 mm and 210 mm, a slightly higher frequency can provide a more effective propulsion force for the caudal fin.

*3.5. Study on Propulsion Performance of Double Caudal Fins in Flow Field.* In many cases, the fish do not swim alone. The caudal fin swing of the former fish will cause the flow field to produce a certain regular wake vortex. The analysis of the way of the caudal fin using the wake vortex energy will be conducive to provide the development of basic theory for underwater biomimetic propulsion.

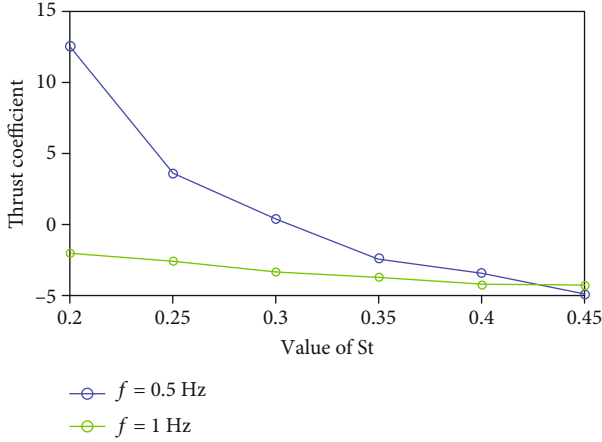


FIGURE 7: The mean value of the force of the caudal fin changes with St number.

Swing frequency, swing amplitude, the phase difference, and the distance between two caudal fins will affect the mutual vortices in the flow field. Among these parameters, the effect of the two caudal fins' angle of attack on the wake vortex is mainly studied. In the process of group swimming, the swimming gait of fish is basically similar. So, we mainly changed the angle of attack during the hydrodynamic numerical simulation analysis, and other parameters are set to the same.

**3.5.1. Simulation Model Establishment.** The flow field is established with a length of 2300 mm and a width of 1000 mm. The distance between the two caudal fins is 250 mm. The caudal fin model and boundary conditions are set to the same as before. The calculation domain creation and meshing are shown in Figure 11.

**3.5.2. Wake Vortex of Double Caudal Fins.** In Figure 12, the double swinging caudal fins have the same swing amplitude in  $A = 150$  mm. The swing frequency is  $f = 0.8$  Hz. And the heaving and pitching movement phase difference is  $60^\circ$ . At  $t = 0.04$  s, the double caudal fins started to move, and the trailing edges of the double caudal fins began to form eddy currents. From  $t = 0.18$  s to  $t = 0.29$  s, the double caudal fins swing simultaneously, and the two vortices formed at the right rear of the double caudal fins gradually converge into a large vortex. Double swinging caudal fins simultaneously sway at  $t = 0.65$  s to  $t = 0.90$  s and form the upper and lower vortices at the trailing edge of caudal fin. At  $t = 1.28$  s, two rows of eddy currents are formed on the lower two sides of the swimming track. Due to the proper spacing and the same swing parameters during the entire swing, the rear caudal fin can add its own vortices to others without destroying the wake vortex of front caudal fin. The superimposed vortex will be beneficial to the rear caudal fins to produce more efficient propulsion.

**3.5.3. Double Caudal Fin Motion Tail Vortex Dissipation Mode.** As shown in Figure 13, when  $t = 0.01$  s, the double caudal fins just started to swing and a wake vortex was

formed at the trailing edge position of the double caudal fins. Between  $t = 0.28$  s and  $t = 0.65$  s, the rear caudal fin swayed with the front one and destroyed the wake vortex formed during the swinging of the front caudal fin. During the latter half of the caudal fin motion (between  $t = 1.03$  s and  $t = 1.35$  s), the wake vortex caused by the swing of the rear caudal fin failed to overlap with the eddy current of the front caudal fin. Due to the difference of angle of attack between double caudal fins, the rear caudal fin will destroy the vortex produced by the front caudal fin, resulting in vortex dissipation that is not conducive to the effective advancement of the rear caudal fin.

## 4. The Control Method of Tail Movement

**4.1. The Analysis of Tail Movement.** The biomimetic tail propulsion mechanism mainly includes the caudal peduncle and the caudal fins. The movement of the caudal fin is driven by the caudal peduncle.

**4.1.1. Caudal Fin Simplified Model.** When biomimetic underwater vehicle is in the process of swimming, the process is shown in Figure 14. Firstly, the static state is shown in Figure 14(a). The caudal fin in the quiescent state does not occur angular swing. Then, as shown in Figure 14(b), the caudal peduncle does not occur swing and the caudal fin begins to swing upward. Subsequently, the caudal peduncle and the caudal fin swing together and the caudal peduncle swings in a large angle as shown in Figure 14(c). Lastly, as shown in Figure 14(d), the caudal peduncle and the caudal fin swing to the initial position from the maximum swing angle. After that, they swing from the equilibrium position to the opposite direction.

**4.1.2. Tail Movement Model Establishment.** The main part of the tail movement part includes the caudal peduncle movement and the caudal fin movement.

In the study of fish tail movement, the caudal fin movement is simplified as a rigid hydrofoil moving in the uniform flow field. The way of movement is around itself doing pitching and heaving swing compound movement. The equation of motion is expressed as follows:

$$\begin{cases} y = A \times \sin(2\pi ft), \\ \theta_1 = \theta_0 \times \sin(2\pi ft - \varphi). \end{cases} \quad (6)$$

We can get the rising-sinking speed along with the Y-axis of caudal fin and the pitching angular velocity around the Z-axis through the derivation of formula (6):

$$V_1 = 2\pi f A \times \cos(2\pi ft), \quad (7)$$

$$\omega = 2\pi f \theta_0 \cos(2\pi ft - \varphi). \quad (8)$$

The half of caudal fin expansion is  $r$ , so the caudal fin swing speed is

$$V = \sqrt{V_1^2 + (\omega r)^2 + 2V_1 \omega r \cos \theta_1}. \quad (9)$$

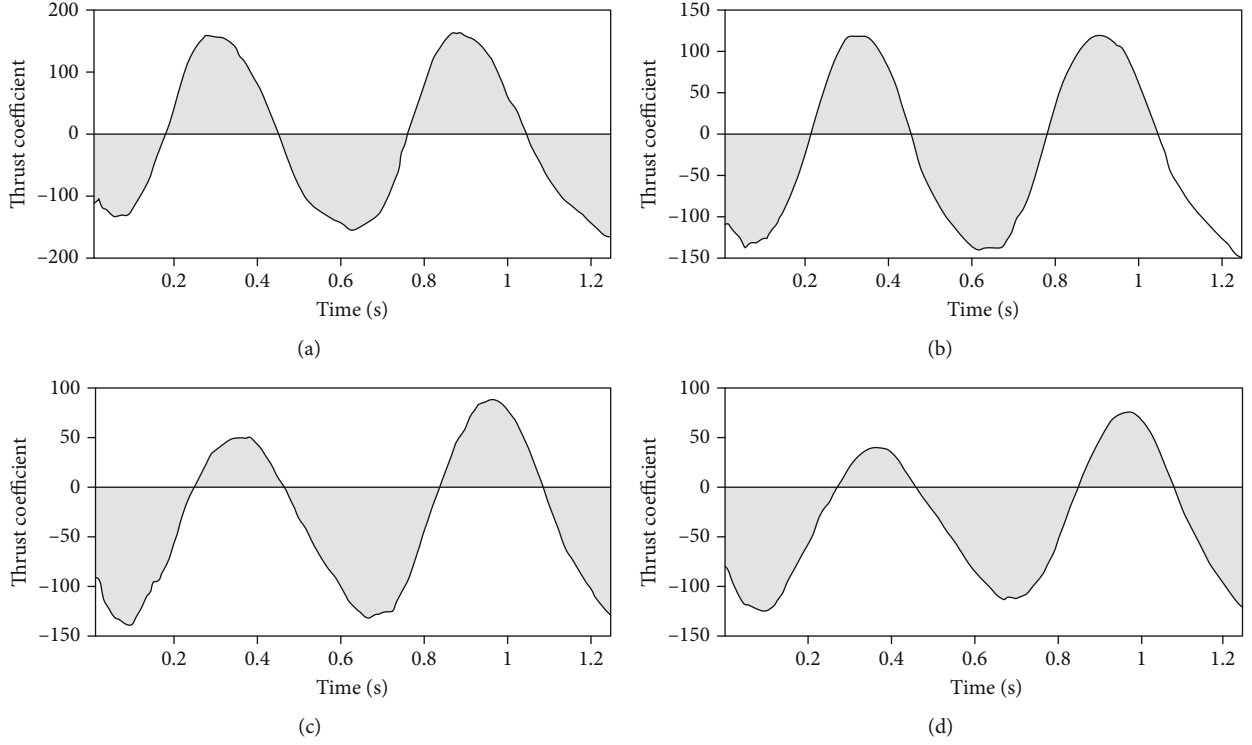


FIGURE 8: Resistance coefficient versus time in a cycle under different phase difference. (a) Phase difference is  $30^\circ$ , angle of attack is  $31.7^\circ$ ; (b) phase difference is  $40^\circ$ , angle of attack is  $28.4^\circ$ ; (c) phase difference is  $50^\circ$ , angle of attack is  $25.6^\circ$ ; (d) phase difference is  $60^\circ$ , angle of attack is  $21.6^\circ$ .

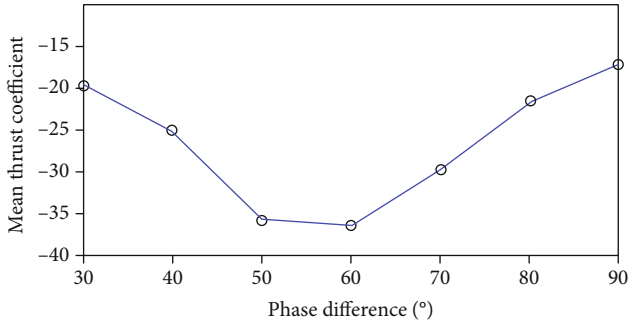


FIGURE 9: Mean thrust coefficient diagram of caudal fin under different phase difference.

Then, we can get the speed of the caudal fin relative to the fluid:

$$\vec{V}_{1t} = \vec{V}_0 + \vec{V}, \quad (10)$$

where  $V_0$  indicates the flow velocity and  $V$  indicates the moving speed of caudal fin along the  $Y$ -axis.

As there is a phase difference  $\phi$  between the caudal peduncle and the caudal fin when they swing, the swing amplitude of caudal peduncle is set as  $A_0$ , so the swing law of caudal peduncle can be expressed as

$$\theta_2(t) = \theta_0 \times \sin(2\pi ft - \phi). \quad (11)$$

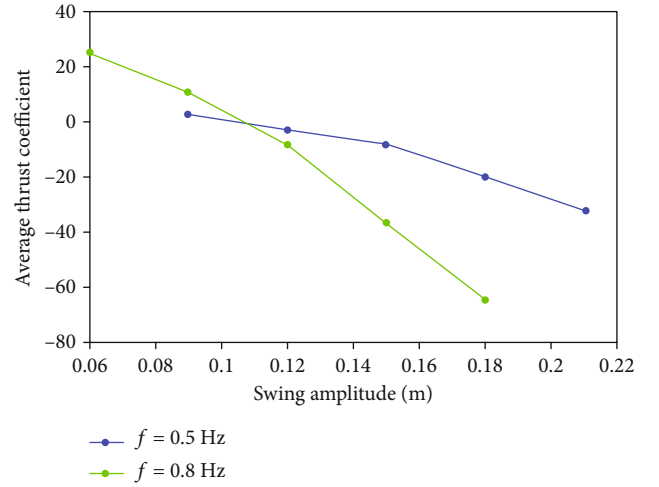


FIGURE 10: Comparison of average thrust coefficient in different swing amplitude.

The swing angular velocity of the caudal peduncle can be expressed by the equation after the derivation of the above formula:

$$\omega_2(t) = 2\pi f \theta_0 \times \cos(2\pi ft - \phi). \quad (12)$$

According to the theory of the wave plate [28], the caudal peduncle movement model can be simplified as a rigid plate. The swing speed of the caudal peduncle can be approximated



FIGURE 11: Calculation domain creation and meshing.

by the linear velocity of the center of gravity of the caudal peduncle. As shown in Figure 15, the distance of caudal peduncle to the fish swing joints is set as  $r_2$ .

When the caudal peduncle is moving in accordance with sinusoidal law, the displacement of the center of gravity can be approximated represented by the following formula:

$$x_2 = r_2 \times \sin \theta_2 = r_2 \times (\theta_0 \times \sin (2\pi ft - \phi)). \quad (13)$$

The speed of the caudal peduncle center of gravity can be expressed as

$$V_2(t) = 2\pi f r_2 \times \theta_0 \times \cos (2\pi ft - \phi). \quad (14)$$

Flow velocity is set as  $V_0$ , so that the relative velocity of the center point of the caudal peduncle is

$$\vec{V}_3(t) = \vec{V}_0 + \vec{V}_2(t). \quad (15)$$

#### 4.2. Establishment of a Kinematic Model of Tail Motion.

When the fish is moving in the flow field, the tail will be subjected to the pressure of the fluid from all directions. The fluid pressure on the surface of the caudal fin is set as  $F_t$ . According to the Bernoulli principle, the analysis of force is as shown in Figure 16.

The propulsive force generated by fluid pressure:

$$F_{t1} = \frac{1}{2} \rho V_{1t}^2 S_1 \sin \theta_1 = \frac{1}{2} \rho S_1 (V_0^2 + 4\pi^2 f^2 A^2 \cos^2(2\pi ft) + \omega^2 r^2 + 2V_1 \omega r \cos \theta_1) \sin \theta_1. \quad (16)$$

According to the wing theory [29, 30], the lift effect on caudal fin is set as  $F$ ; the stress analysis is shown in Figure 16.

The lift force of the fluid on the caudal fin in the vertical direction of the caudal fin is

$$F_s = 2\pi \rho L C V_{1t}^2 \sin \alpha \cos \alpha, \quad (17)$$

where  $\alpha$  is the instantaneous relative angle of attack of the caudal fin;

$$\begin{aligned} \alpha &= \arctg\left(\frac{V_{1t}}{V_0} + \theta_1\right) \\ &= \arctg\left(\frac{4\pi^2 f^2 A^2 \cos^2(2\pi ft) + \omega^2 r^2 + 2V_1 \omega r \cos \theta_1}{V_0} + \theta_1\right), \end{aligned} \quad (18)$$

where  $\theta_1$  is the instantaneous swing angle of the caudal fin,  $L$  is the length of slender, and  $C$  is the chord length.

The driving force produced by the lifting of the caudal fin is

$$\begin{aligned} F_{s1} &= 2\pi \rho L C V_{1t}^2 \sin \alpha \cos \alpha \sin \theta_1 \\ &= 2\pi \rho L C (V_0^2 + 4\pi^2 f^2 A^2 \cos^2(2\pi ft) + \omega^2 r^2 \\ &\quad + 2V_1 \omega r \cos \theta_1) \sin \alpha \cos \alpha \sin (\theta_0 \times \sin (2\pi ft - \phi)). \end{aligned} \quad (19)$$

From the above analysis, we can obtain the total propulsion produced by the moving caudal fin:

$$\begin{aligned} F_1 &= F_{t1} + F_{s1} = \frac{1}{2} \rho S_1 (V_0^2 + 4\pi^2 f^2 A^2 \cos^2(2\pi ft) + \omega^2 r^2 \\ &\quad + 2V_1 \omega r \cos \theta_1) \sin \theta_1 + 2\pi \rho L C (V_0^2 \\ &\quad + 4\pi^2 f^2 A^2 \cos^2(2\pi ft) + \omega^2 r^2 \\ &\quad + 2V_1 \omega r \cos \theta_1) \sin \alpha \cos \alpha \sin (\theta_0 \times \sin (2\pi ft - \phi)). \end{aligned} \quad (20)$$

The analysis and calculation of the propulsion is similar to that of the caudal fin. The total propulsion calculation method of the caudal peduncle can be expressed as follows:

$$\begin{aligned} F_2 &= \frac{1}{2} \rho (V_0^2 + 4\pi^2 f^2 r_2^2 \times \theta_0^2 \times \cos^2(2\pi ft - \phi)) \\ &\quad \times S_2 \times \sin \theta_2 + 2\pi \rho L C (V_0^2 + 4\pi^2 f^2 r_2^2 \times \theta_0^2 \\ &\quad \times \cos^2(2\pi ft - \phi)) \sin \alpha_2 \cos \alpha_2 \sin (\theta_0 \times \sin (2\pi ft - \phi)). \end{aligned} \quad (21)$$

#### 4.3. Gait Fitting of Fish Body Tail Biomimetic Mechanism.

In Section 4, we used the link mechanism to simulate the fish body wave, so it is necessary to control the swing angle of each joint in order that each connection endpoint can approximately fit the fish wave curve. The  $\lambda$  is defined as the ratio of the length of the tail swing to the whole wavelength. It is essential to ensure that each linkage is continuous and the end point is at the end of the last linkage on the fish body wave curve. The end position of linkage satisfies the following equations:

$$\begin{cases} (x_{i,j} - x_{i,j-1})^2 + (y_{i,j} - y_{i,j-1})^2 = L_j^2, \\ y_{i,j}(x, t) = (c_1 x_i + c_2 x_i^2) \sin \left( kx_i - \frac{2\pi}{M} i \right), \end{cases} \quad (22)$$



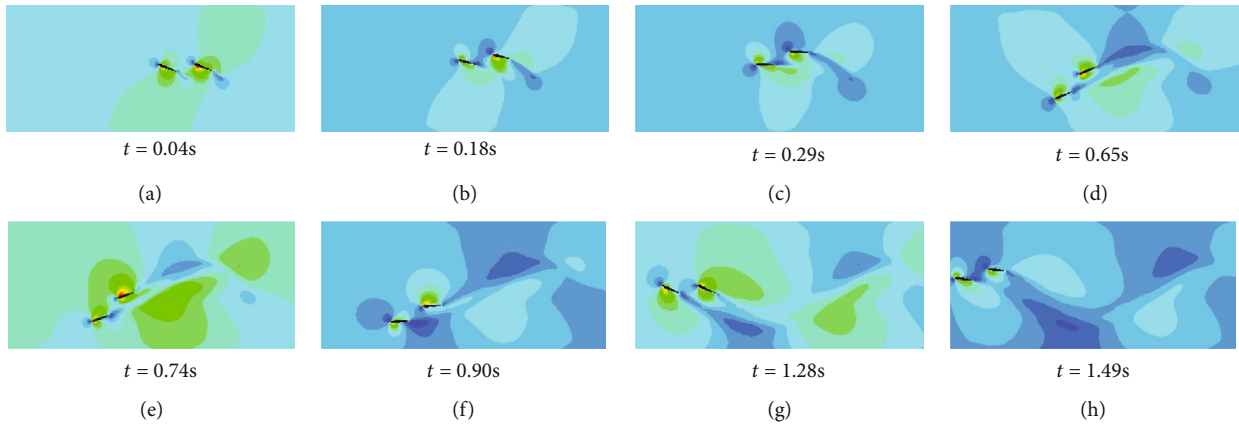


FIGURE 12: Wake vortex of double caudal fin pressure cloud.

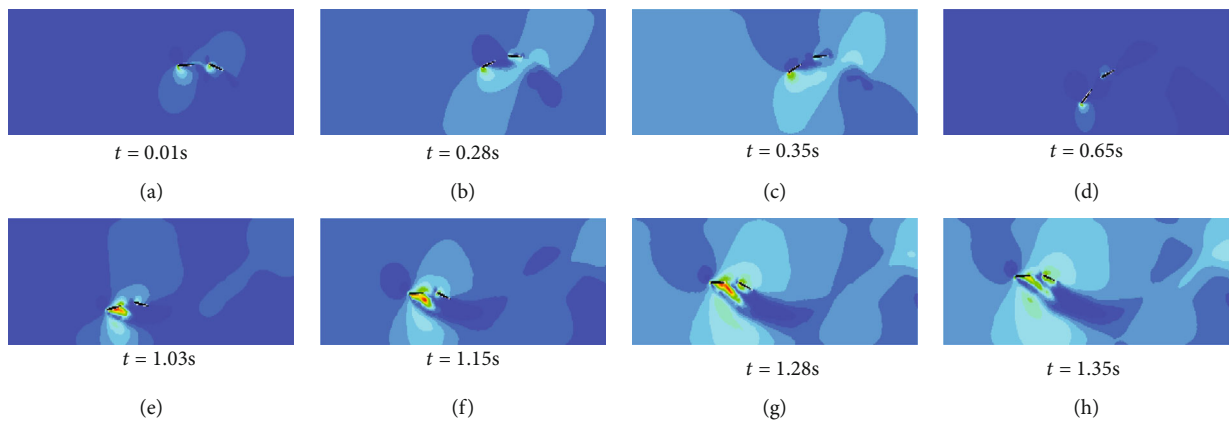


FIGURE 13: Vortex's dissipation model pressure cloud.

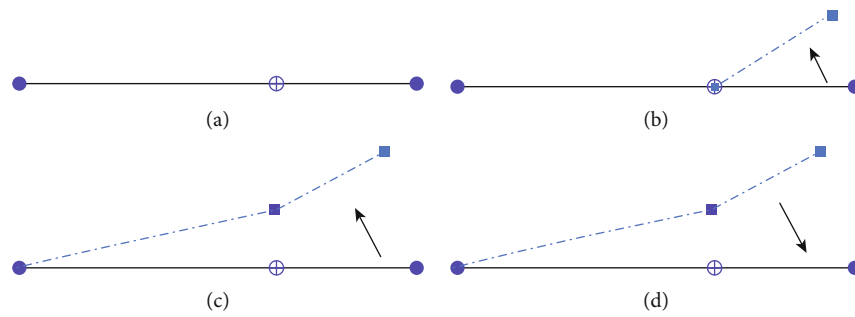


FIGURE 14: Tail swing diagram.

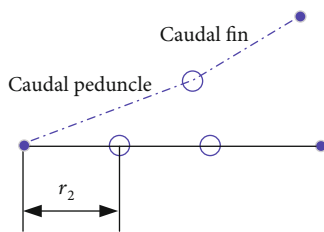


FIGURE 15: Schematic diagram of caudal peduncle swing.

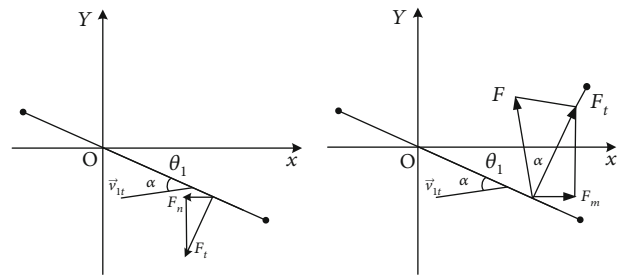


FIGURE 16: Schematic diagram of the caudal fin's fluid pressure decomposition and lift force analysis.

where  $(x_{i,j}, y_{i,j})$  is the angular coordinate of the “ $j$ ” linkage at the moment  $i$  in the swing period,  $x_{i,0} = 0$ ,  $x_{i,5} = \lambda \cdot 2\pi$ ,  $1 \leq j \leq 5$ ,  $0 \leq i \leq M$ .

Bring  $L_j$  into the formula (23), we can solve the coordinates of each endpoint at  $i = 0$ ,  $i = 1$  until  $i = M$ . After that, we can get the angle  $\theta_{i,j}$  between each linkage and fish body, which can be expressed as

$$\theta_{i,j} = \arctan \left[ \frac{x_{i,j} - x_{i,j-1}}{y_{i,j} - y_{i,j-1}} \right]. \quad (23)$$

The swing angles of the five steering gears are calculated, respectively,

$$\begin{cases} \varphi_1 = \arctan \left( \frac{y_1 - y_0}{x_1 - x_0} \right), \\ \varphi_2 = \arctan \left( \frac{y_2 - y_1}{x_2 - x_1} \right) - \varphi_1, \\ \varphi_3 = \arctan \left( \frac{y_3 - y_2}{x_3 - x_2} \right) - \varphi_2, \\ \varphi_4 = \arctan \left( \frac{y_4 - y_3}{x_4 - x_3} \right) - \varphi_3, \\ \varphi_5 = \arctan \left( \frac{y_4 - y_3}{x_4 - x_3} \right) - \varphi_4. \end{cases} \quad (24)$$

Through the analysis of the fish body wave function, we can obtain that as the number of joints increases, it is easier to fit the fish body wave curve, but it is more difficult to coordinate control between the steering gear (the motion of the tail swing is controlled by the steering gear). Thus, the endpoints of the five joints should be fitted to the corresponding fish body wave curve as much as possible. More importantly, the working angle of each steering gear and their mutual position relationship should be well controlled. In this way, the bionic underwater vehicle can be moved like a fish, thus improving the propulsion efficiency and saving energy.

## 5. Conclusion

In this paper, the fast-moving swordfish was taken as the research object to explore the flow field structure of the swordfish caudal fin swinging. The mechanism of the caudal fin propulsion was preliminarily investigated, and the bionic mechanism motion fitting was carried out. The main conclusions were obtained as follows:

- (1) During the swinging process, the fish-tail forms a wake vortex due to the transformation of the high-pressure and low-pressure zones. The tangential direction of the body vortex at the  $X$ -axis position is opposite to the swimming direction of the caudal fin, thereby forming a backward jet in the tail flow field, which produces a forward thrust

- (2) When St number is in the range of 0.25 to 0.45, the propulsive force generated by the caudal fin in one swing period gradually increases as the St number increases, but the range of the increasing amplitude gradually becomes smaller. In addition, when the phase difference is in the range of  $50^\circ \sim 60^\circ$ , the propulsion of the caudal fin is relatively large and this is a more optimized motion mode
- (3) For hydrodynamic studies of double caudal fins, changing the angle of attack of the double caudal fins will produce different wake flow field structures. A reasonable use of the wake vortex generated by the front caudal fin will help the rear caudal fin to reduce the resistance and generate a propulsive force more effectively
- (4) By studying the motion law of the tail of swordfish, the motion fitting of the tail swing was carried out by using the link mechanism which was widely used in machinery. By calculating the thrust of the simplified tail swing model, the principle of the thrust generated by the caudal fin and caudal peduncle in the process of propulsion was analyzed. By controlling the angle of the steering gear, the fish body wave was fitted to the fish tail motion. In this way, the biomimetic motion mechanism of the caudal fin was preliminarily studied

## 6. Future Work

Based on the present study on theoretical calculation analysis of the caudal fin, the authors will build an experimental platform for the experimental analysis of the swing angle of the caudal fin by using the linkage mechanism, which further verifies the correctness of our simulation results in the future work.

## Data Availability

The data used to support the findings of this study are available from the corresponding author upon request.

## Conflicts of Interest

The authors declare that there is no conflict of interest regarding the publication of this paper.

## Acknowledgments

This research was supported by the National Science Foundation of China (No. 61540010 and No. 51979259) and the Shandong Natural Science Foundation (No. ZR201709240210).

## References

- [1] F. Liu, Y. Shen, B. He et al., “Drift angle compensation-based adaptive line-of-sight path following for autonomous underwater vehicle,” *Applied Ocean Research*, vol. 93, article 101943, 2019.

- [2] A. Raj and A. Thakur, "Fish-inspired robots: design, sensing, actuation, and autonomy—a review of research," *Bioinspiration & Biomimetics*, vol. 11, no. 3, article 031001, 2016.
- [3] T. Y. T. Wu, "Hydromechanics of swimming propulsion. Part 1. Swimming of a two-dimensional flexible plate at variable forward speeds in an inviscid fluid," *Journal of Fluid Mechanics*, vol. 46, no. 2, pp. 337–355, 1971.
- [4] A. Wang, G. Liu, X. Wang, and B. Fu, "Development and analysis of body and/or caudal fin biomimetic robot fish," *Journal of Mechanical Engineering*, vol. 52, no. 17, pp. 137–146, 2016.
- [5] M. J. Lighthill, "Aquatic animal propulsion of high hydro-mechanical efficiency," *Journal of Fluid Mechanics*, vol. 44, no. 2, pp. 265–301, 1970.
- [6] M. J. Lighthill, "Large-amplitude elongated-body theory of fish locomotion," *Proceedings of the Royal Society of London. Series B. Biological Sciences*, vol. 179, no. 1055, pp. 125–138, 1997.
- [7] F. Candelier, F. Boyer, and A. Leroyer, "Three-dimensional extension of Lighthill's large-amplitude elongated-body theory of fish locomotion," *Journal of Fluid Mechanics*, vol. 674, pp. 196–226, 2011.
- [8] G. I. Taylor, "Analysis of the swimming of long and narrow animals," *Proceedings of the Royal Society of London. Series A. Mathematical and Physical Sciences*, vol. 214, no. 1117, pp. 158–183, 1997.
- [9] R. G. Root and C. W. Liew, "Computational and mathematical modeling of the effects of tailbeat frequency and flexural stiffness in swimming fish," *Zoology*, vol. 117, no. 1, pp. 81–85, 2014.
- [10] Q. Zhu and X. Bi, "Effects of stiffness distribution and spanwise deformation on the dynamics of a ray-supported caudal fin," *Bioinspiration & Biomimetics*, vol. 12, no. 2, article 026011, 2017.
- [11] L. B. Pon, S. G. Hinch, G. N. Wagner, A. G. Lotto, and S. J. Cooke, "Swimming performance and morphology of juvenile sockeye salmon, *Oncorhynchus nerka*: comparison of inlet and outlet fry populations," *Environmental Biology of Fishes*, vol. 78, no. 3, pp. 257–269, 2007.
- [12] Z. Ren, X. Yang, T. Wang, and L. Wen, "Hydrodynamics of a robotic fish tail: effects of the caudal peduncle, fin ray motions and the flow speed," *Bioinspiration & Biomimetics*, vol. 11, no. 1, article 016008, 2016.
- [13] D. Yun, K. S. Kim, and S. Kim, "Thrust characteristic of a caudal fin with spanwise variable phase," *Ocean Engineering*, vol. 104, pp. 344–348, 2015.
- [14] B. Liu, S. Zhang, F. Qin, and J. Yang, "Fluid–structure interaction study on the performance of flexible articulated caudal fin," *Advanced Robotics*, vol. 28, no. 24, pp. 1665–1676, 2014.
- [15] Z. Xin and C. Wu, "Shape optimization of the caudal fin of the three-dimensional self-propelled swimming fish," *Science China Physics, Mechanics and Astronomy*, vol. 56, no. 2, pp. 328–339, 2013.
- [16] T. Tomita, M. Toda, K. Miyamoto, S. I. Oka, K. Ueda, and K. Sato, "Development of the lunate-shaped caudal fin in white shark embryos," *The Anatomical Record*, vol. 301, no. 6, pp. 1068–1073, 2018.
- [17] B. E. Flammang and G. V. Lauder, "Caudal fin shape modulation and control during acceleration, braking and backing maneuvers in bluegill sunfish, *Lepomis macrochirus*," *Journal of Experimental Biology*, vol. 212, no. 2, pp. 277–286, 2008.
- [18] L. Wen, T. Wang, G. Wu, and J. Liang, "Quantitative thrust efficiency of a self-propulsive robotic fish: experimental method and hydrodynamic investigation," *IEEE/ASME Transactions on Mechatronics*, vol. 18, no. 3, pp. 1027–1038, 2013.
- [19] X. Yin, L. Jia, C. Wang, and G. Xie, "Modelling of thrust generated by oscillation caudal fin of underwater bionic robot," *Applied Mathematics and Mechanics*, vol. 37, no. 5, pp. 601–610, 2016.
- [20] Y. Zhong, Z. Li, and R. Du, "Robot fish with two-DOF pectoral fins and a wire-driven caudal fin," *Advanced Robotics*, vol. 32, no. 1, pp. 25–36, 2017.
- [21] J. Yu, M. Tan, S. Wang, and E. Chen, "Development of a biomimetic robotic fish and its control algorithm," *IEEE Transactions on Systems, Man and Cybernetics, Part B (Cybernetics)*, vol. 34, no. 4, pp. 1798–1810, 2004.
- [22] T. Nguyen, L. White, R. Vaghetto, and Y. Hassan, "Turbulent flow and vortex characteristics in a blocked subchannel of a helically wrapped rod bundle," *Experiments in Fluids*, vol. 60, no. 8, article 129, 2019.
- [23] M. Wei and L. Yang, *Computational Fluid Dynamics*, Education Science Press, Beijing, China, 1985.
- [24] X. Zhang, Y. Su, and Z. Wang, "Numerical and experimental studies of influence of the caudal fin shape on the propulsion performance of a flapping caudal fin," *Journal of Hydrodynamics*, vol. 23, no. 3, pp. 325–332, 2011.
- [25] P. Coste and J. Lavieville, "A turbulence model for large interfaces in high Reynolds two-phase CFD," *Nuclear Engineering and Design*, vol. 284, pp. 162–175, 2015.
- [26] S. Ovtchinnikov, F. Dobrian, X. C. Cai, and D. E. Keyes, "Additive schwarz-based fully coupled implicit methods for resistive hall magnetohydrodynamic problems," *Journal of Computational Physics*, vol. 225, no. 2, pp. 1919–1936, 2007.
- [27] P. Liao, S. Zhang, and D. Sun, "A dual caudal-fin miniature robotic fish with an integrated oscillation and jet propulsive mechanism," *Bioinspiration & Biomimetics*, vol. 13, no. 3, article 036007, 2018.
- [28] N. Kato, "Median and paired fin controllers for biomimetic marine vehicles," *Applied Mechanics Reviews*, vol. 58, no. 4, pp. 238–252, 2005.
- [29] A. Khanjian, C. Habchi, S. Russeil, D. Bougeard, and T. Lemenand, "Effect of the angle of attack of a rectangular wing on the heat transfer enhancement in channel flow at low Reynolds number," *Heat and Mass Transfer*, vol. 54, no. 5, pp. 1441–1452, 2018.
- [30] O. J. Boelens, "CFD analysis of the flow around the X-31 aircraft at high angle of attack," *Aerospace Science and Technology*, vol. 20, no. 1, pp. 38–51, 2012.